Aerodynamic Analysis of a Three-Bladed Pivoted Savonius Wind Turbine: Wind Tunnel Testing and Numerical Simulation

M. Amiri [1], M. Kahrom[2†] and A. R. Teymourtash[2]

[1] *Department of Energy Engineering, Quchan University of Technology, Quchan, Iran*
[2] *Department of Mechanical Engineering, Ferdowsi University of Mashhad, Mashhad, Iran*

†*Corresponding Author Email: mkahrom@um.ac.ir*

ABSTRACT

In this study, a three-bladed pivoted vertical axis Savonius wind turbine is subjected to numerical and experimental studies. The experiments are carried out in a subsonic open-jet type wind tunnel, where the instantaneous position of the opening/closing blades are also determined via high speed imaging. The effects of adding end plates and the rotor aspect ratio on the turbine torque and power coefficients are investigated experimentally. Results show that adding end plates greatly enhances the rotor aerodynamic performance, in terms of both the maximum power coefficient and also the working range of the turbine. Similar effects are also observed for the effects of increasing the aspect ratio. Comparing numerical results with the experimental data demonstrated that the numerical results are in a convincing agreement with the experimental data of a wind rotor with an aspect ratio of 2.0 equipped with end plates. Although there are several two-dimensional numerical simulations for the drag-based vertical axis wind turbines in the literature, the results of the current study suggests that two-dimensional numerical results are not comparable with the experimental data of the rotors with small aspect ratios, especially without end plates.

Keywords: Pivoted savonius; Aspect ratio; End plate; Multiple reference frame; Vertical axis.

NOMENCLATURE

AR	aspect ratio	R_t	distance between the drum axis and the tip of the fully-opened blade
C_P	power coefficient		
C_M	torque coefficient	Re	Reynolds number
D	drum diameter	TSR	Tip Speed Ratio
$\vec{F}_P$	pressure force vector	T	torque
$\vec{F}_v$	viscos force vector	U	free stream velocity
H	drum height	u_r	moving frame velocity
$\vec{M}_A$	total moment vector		
p	pressure	v_r	relative velocity
$\vec{r}_{AB}$	position vector	v	absolute velocity
r	position vector	θ	rotational angle
R_c	distance between the drum axis and the center of the fully-opened blade chord	μ	air viscosity
		ρ	air density
		$\bar{\bar{\tau}}$	stress tensor
		ω	rotational speed

1. INTRODUCTION

Wind energy as one of the most remarkable renewable power resources, has more than two thousand years of history. In the recent three decades, the wind turbines have again started to spread all over the globe, due to the energy crisis (Roy and Saha 2013a). The main component of a wind energy conversion system is the wind turbine, which can be classified based on its rotation axis alignment to horizontal axis wind turbines (HAWTs) and vertical axis wind turbines (VAWTs) (Tang *et*

al., 2013). Among the VAWTs, Savonius rotor is popular due to its simple design and manufacture. It is a drag driven wind rotor having two, three or more semicircular cylindrical blades. High starting torque, easy fabrication and installation and the ability to receive wind from all directions are its most noticeable advantages (Duffett *et al.*, 2009). However, Savonius rotor suffers from a low energy absorption efficiency, which has been the motivation for numerous investigations. (Roy and Saha 2013b) numerically investigated the effects of overlap ratio on the static torque characteristics of a conventional two-bladed Savonius rotor. They concluded that an overlap ratio of 0.2 provides the minimum angular variations of the static torque and eliminates the negative static torque.(Kianifar and Anbarsooz 2011) examined the blade curve effects on the power coefficient of a Savonius rotor with two blades at various overlap ratios. Their experimental and numerical findings showed that the semi-circular blade having an overlap ratio of 0.2 exhibits a superior power coefficient among others. (Alexander and Holownia 1978) showed that the existence of end-plates can greatly increase the absorption efficiency of Savonius rotors, because the end plates do not let the air escape from the concave side of the buckets. (Hayashi *et al.* 2005) suggested multiple stage two-bucket rotors to reduce the fluctuations of the output torque. Since the stages were assembled with a phase shift, the rotor had no negative static torque. Helical Savonius rotors have also been proposed to improve the rotor starting torque. (Kamoji *et al.*, 2009) experimentally tested the aerodynamic performance of a two-bladed helical rotor with 90 degrees twist angle at several aspect ratios and overlap ratios. They concluded that the power coefficient of a shaft-less rotor, with an aspect ratio of 0.88 and zero overlap ratio, almost equals to that of a conventional rotor with an aspect ratio of 1.0. Nevertheless, the helical rotor has no negative starting torque. Similarly, (Anbarsooz 2016) studied helical rotors with 30 and 45 degrees twist angles and revealed that although the helical rotors have exhibited a more uniform output torque, the maximum efficiency of the helical rotors are slightly lower than that of the conventional rotor.(Ricci *et al.* 2016) analyzed the effects of several construction solutions on the power coefficient of a Savonius rotor which was employed in a lamppost. Their results showed that Reynolds number does not have significant effects on the rotor performance, however, the blades overlap and adding end plates can enhance the rotor performance. Furthermore, the presence of external grids and structural posts deteriorates the rotor power coefficient.(Tian *et al.* 2018) employed a Particle Swarm Optimization (PSO) algorithm to optimize the power coefficient of a novel Savonius rotor with different concave and convex sides. The power coefficient of the modified rotor is 4.41% higher than that of the conventional rotor. (Chan *et al.* 2018) also utilized the genetic algorithm in conjunction with the computational fluid dynamic simulations to find the optimal blade shape of the Savonius rotor. They succeeded to reach a 33% increment in the time-averaged power coefficient of the turbine, compared to the Savonius rotor with semicircular blades.

The main reason for the low absorption efficiency of the Savonius rotor is the negative torque of the returning blade. In order to minimize this undesired torque, (Saha *et al.* 2008) devised a valve on the rotor blades which is open when the wind is blowing on the convex side of the blade and it is closed otherwise. They succeeded to reach a 7% increase in the maximum power coefficient of the rotor in their experiments. (Altan and Atılgan 2010) proposed a curtain in front of a Savonius rotor to prevent the upcoming wind from reaching the returning blade which is producing the negative torque. Although this method can efficiency guide and accelerate the wind towards the advancing blade and reduces the negative torque, it makes the rotor to be sensitive to the wind direction and the rotor is no longer omnidirectional.

A novel design which minimized the negative torque of the returning blades and at the same time, preserves the omnidirectional characteristics of the rotor is using pivoted blades (Yang and Lawn, 2011; Amiri *et al.,* 2016). In this design, the blades which are pivoted to a drum, cannot resist a negative torque and they will be closed. However, when the blades are opened by the incident wind, they would encounter some stops and will be held in their fully-opened position. (Yang and Lawn 2011) employed such a turbine for tidal currents or fast flowing streams. They provided some simplified basic rules for the opening/closing processes of each blade, based on experimental observations. Furthermore, they performed two-dimensional quasi-steady CFD simulations and presented a polynomial function for the effective force coefficient acting on each blade as a function of the rotational angle and the flow coefficient. (D'Alessandro *et al*. 2010) verified that, the presence of end plates confine the three-dimensional flow characteristics around the rotor tips which allows comparing experimental results of three-dimensional models to two-dimensional numerical data. For this reason, there are various two-dimensional numerical studies on vertical axis wind turbines (Emmanuel and Jun, 2011; Torresi *et al.,* 2011, Nasef *et al.,* 2013, El-Askary *et al.*, 2015) . (Amiri *et al.,* 2016) employed pivoted rotors for wind energy production for the first time. They studied the effects of blade numbers on the rotor power coefficient, experimentally and numerically and revealed that the pivoted rotor has no negative torque in one complete revolution. Their results also showed that although the 6-bladed rotor has a more uniform output torque, the maximum power coefficient of a 3-bladed rotor is larger and reaches 0.21. Their two-dimensional numerical simulations were performed using the multiple reference frame model (MRF), which is based on the quasi-steady assumption.

The main aim of the current research is to further improve the energy conversion efficiency of the above-mentioned 3-bladed pivoted wind turbine. In this regard, the effects of the rotor aspect ratio and the presence of end plates on the power and torque coefficients of the rotor are examined experimentally in an open-jet type wind tunnel. Furthermore, the

effects of the number of angular positions required to accurately capture one complete revolution of the rotor are investigated. In this regard, the geometry variations of the rotor in one complete revolution are determined using high speed imaging and the corresponding numerical simulations are performed considering two different number of the angular positions.

2. SCHEMATIC OF A THREE-BLADED ROTOR

The geometrical parameters of a 3-bladed rotor are shown in Fig. 1, where D is the diameter of the drum, R_c the distance between the center of the fully opened blade chord and the drum axis and R_t is the distance between the tip of the fully-opened blade and the drum axis. The rotational angle, θ, is measured from the incident wind direction and indicates the rotational angle of the hinge point of Blade 1.
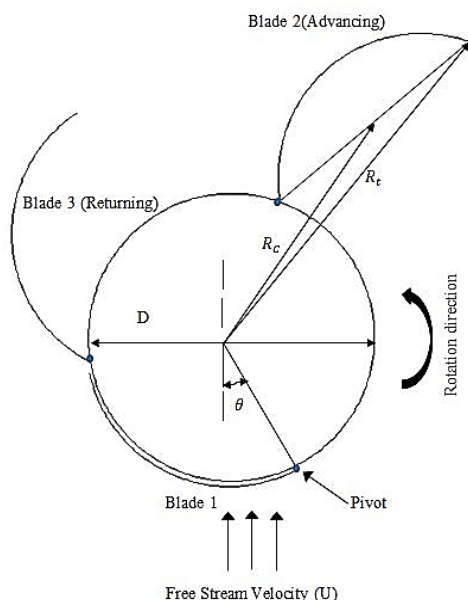

Fig. 1. Geometrical parameters of a 3-bladed rotor.

In one complete rotor rotation, each blade undergoes two dynamic processes; the opening and the closing processes. In the current study, high speed imaging is performed on a 3-bladed rotor which is tested in a wind tunnel and the instance of the opening/closing processes are determined. The details of the experimental setup are given in the next Section.

3. EXPERIMENTAL SETUP

A low-speed open-circuit type wind tunnel is used for the experimental measurement. The test section of the wind tunnel is a 600×600 *mm* square cylinder having a length of 2000 *mm*, available at Ferdowsi University of Mashhad (Amiri *et al*. 2016). The assembly of the wind turbine and the torque measuring setup are placed 300 *mm* downstream of the tunnel exit, as shown in Fig. 2. In order to apply

the desired mechanical torques to the tested turbines, a pulley which is attached to the turbine is used. As shown in Fig. 3, the pulley is connected to two load cells via a pulley. The pulley rotates with the shaft, while the rope is fixed. Therefore, a frictional force exists between the rope and pulley. The difference between the values of the load cells equals this frictional force. The braking torque applied on the turbine equals this frictional force multiplied by the radius of the pulley. Three-bladed rotors with the aspect ratios of 1, 1.5 and 2.0, which are made up of 0.4-*mm*-thick galvanized iron, are considered for the experiments and shown in Fig. 4. A schematic of the rotor with endplates is presented in Fig. 5. The drum diameter for all the rotors is 160 *mm*. The geometrical parameters of the tested rotors are given in Table 1, where H is the drum height.

Table 1 Geometrical parameters of the tested turbines

Rotor Type	D (*mm*)	H (*mm*)	R_c (*mm*)	R_t (*mm*)
1	160	160	144	211
2	160	240	144	211
3	160	320	144	211

A blade anemometer of the type Lutron AM-4200, used for measuring the wind speed. The accuracy of the anemometer was 0.1 *m/s* with an operating range of 0.8 – 30 *m/s*. The rotor rotational speed, however, was measured via an optical tachometer of the type Compact Instruments CT6/LSR, with an operating range of 3 – 99999 *rpm* and an accuracy of 0.05%. High-speed imaging is performed using a SONY A6300 camera, with a frame rate of 120 fps.

In order to evaluate the rotor blockage effects on the measured experimental data, the methodology introduced by (Roy and Saha 2015) is employed. It has been shown that this method is suitable for open-jet type wind tunnel experiments (Roy and Saha 2015, Anbarsooz 2016). The sequential perturbation technique proposed by Moffat (Moffat 1982, Moffat 1988) is employed for the uncertainty analysis of the experimental data. The resultant maximum uncertainties are given in Table 2 for the main parameters of the current study.

Table 2 The uncertainties for the main measured parameters of the experimental measurements

Parameter Uncertainty	(%)
Wind velocity	1.18
Diameter	0.18
Tip speed ratio	2.8
torque Coefficient	4.6
power Coefficient	5.1

4. GOVERNING EQUATIONS AND NUMERICAL METHOD

In this study, the multiple reference frame (MRF) model is used to evaluate the turbine rotation effects on the flow field. In this method, which is also

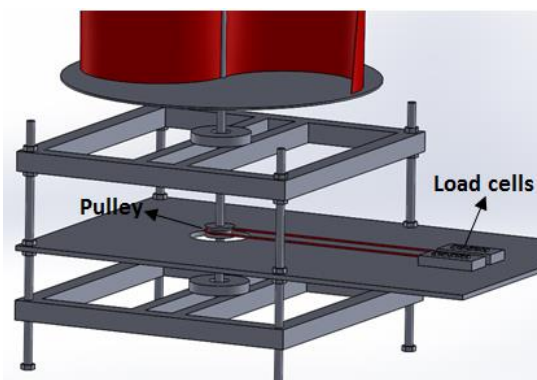**Fig. 2. Experimental setup at Ferdowsi University of Mashhad.**

Fig. 3. Schematic of the torque measuring device.

Fig. 4. 3-bladed rotors with various aspect ratios used in the experimental measurements.

known as the 'frozen rotor approach', the simulations are performed based on a quasi-steady assumption (Pope *et al.* 2010). In the MRF approach, instead of performing simulations with rotating and dynamic grids, the mesh remains fixed and the simulation is performed at several angular positions in a full rotation. In fact, in this method the motion of the turbine is frozen in a specific position and the instantaneous flow field around the rotor in that specific rotation is determined. This is why this method has been called "the frozen rotor approach". In this regard, the computational domain is separated into two subdomains: a rotating zone around the rotor and a stationary zone, as shown in Fig. 6. In this figure, the applied boundary conditions and also the size of the computational domain are specified. The simulations are performed at several angular positions of the rotor at every desired rotational speed. The desired rotational speed, $\vec{\omega}$, is assigned to the rotating zone. The applicability of the MRF model in numerical simulation of the vertical axis wind turbines has also been verified by various researchers (Pope et al. 2010; Ghatage and Joshi 2012; Kang *et al.* 2014). The two-dimensional governing equations of an incompressible Newtonian fluid flow, in the MRF model, over a rotating zone, can be written as Eqs. (1) and (2) (Pope *et al.* 2010):
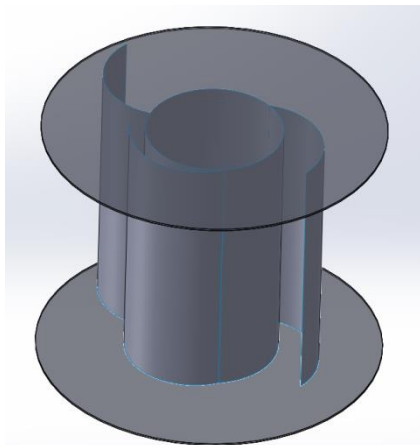

Fig. 5. A schematic of the rotor with endplates.

$$\nabla.\rho\vec{v}_r = 0 \tag{1}$$

$$\nabla.\left(\rho\vec{v}_r\vec{\upsilon}\right) + \rho\left(\vec{\omega}\times\vec{\upsilon}\right) = -\nabla p + \nabla.\bar{\bar{\tau}} + \rho\vec{g} \tag{2}$$

where, $\vec{\upsilon}$ is the absolute velocity and $\vec{v}_r$ is the relative velocity, as given in Eq. (3):

$$\vec{v}_r = \vec{\upsilon} - \vec{u}_r \tag{3}$$

where $\vec{u}_r$ is the moving frame velocity. In this study, the moving frame velocity is the rotational velocity of the rotating zone, which can be written as Eq. (4):

$$\vec{u}_r = \vec{\omega}\times\vec{r} \tag{4}$$

where $\vec{r}$ is the position vector, calculated from the origin of the rotating zone. In the MRF approach, the simulations are performed in several angular

positions of the rotor and in each position the simulation iss performed in a steady condition.

Second-order Upwind scheme is used for discretization of the momentum, turbulent kinetic energy and turbulent dissipation rate transport equations.

The convergence criterion for the continuity equation is considered 10^{-3} and for the momentum equations, turbulent kinetic energy and turbulent dissipation rate transport equations are 10^{-6}.
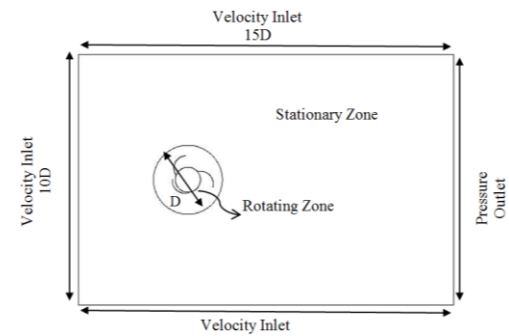

Fig. 6. Computational domain and the boundary conditions.

The moment vector, $\vec{M}_A$, about the rotor center, O, is obtained by summing the cross products of the pressure and viscous force vectors $(\vec{F}_P, \vec{F}_v)$ for all the computational faces on the blades with the corresponding position vector, $\vec{r}_{OB}$.

$$\vec{M}_O = \vec{r}_{OB}\times\vec{F}_P + \vec{r}_{OB}\times\vec{F}_V \tag{5}$$

The position vector is a vector from the rotor center to the force origin (Inc. 2009).

In order to consider the turbulence effects on the aerodynamic performance of the rotor, the SST k-ω turbulence model is employed. Several researchers have certified the suitability of this turbulence model when it is employed with the MRF model for numerical simulation of vertical axis wind turbines (Lanzafame *et al.* 2013, El-Askary *et al.* 2015).

The effects of the grid size on the output power of the rotor had been investigated in a previous paper (Amiri *et al.* 2016) and they are not repeated here. The results of the mesh-independency study, revealed that an unstructured grid having nearly 223,000 cells, is the most proper grid. The resolution of this grid around the rotor blades is depicted in Fig. 7. The value of y⁺ which has been averaged over the rotor blades did not exceed 1.47 for all the numerical simulations performed in this study.

5. RESULTS AND DISCUSSION

As stated before, the blades of the proposed turbine are pivoted to the drum and alternatively opened and closed in a complete rotor revolution. In the numerical simulation of the turbine, it is necessary to determine the status of the blades (whether fully-opened, fully-closed or in the opening/closing process) at each angular position. (Yang and Lawn 2011) performed
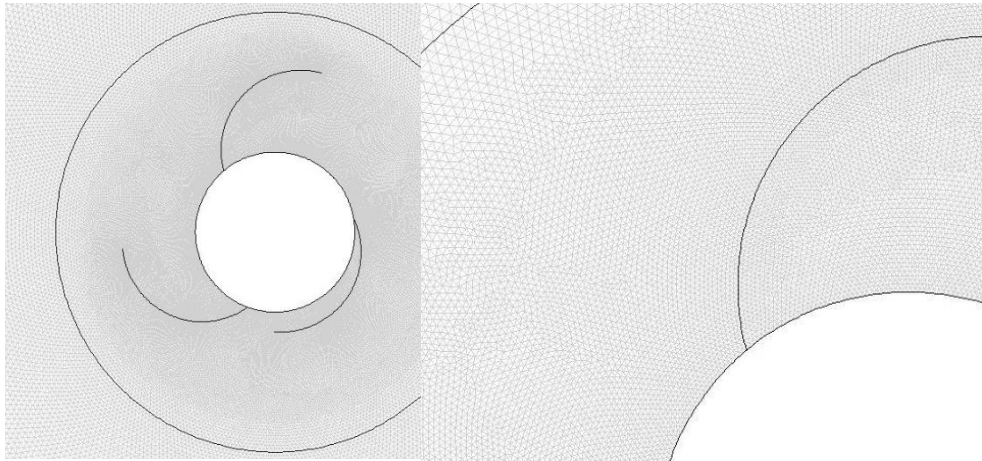
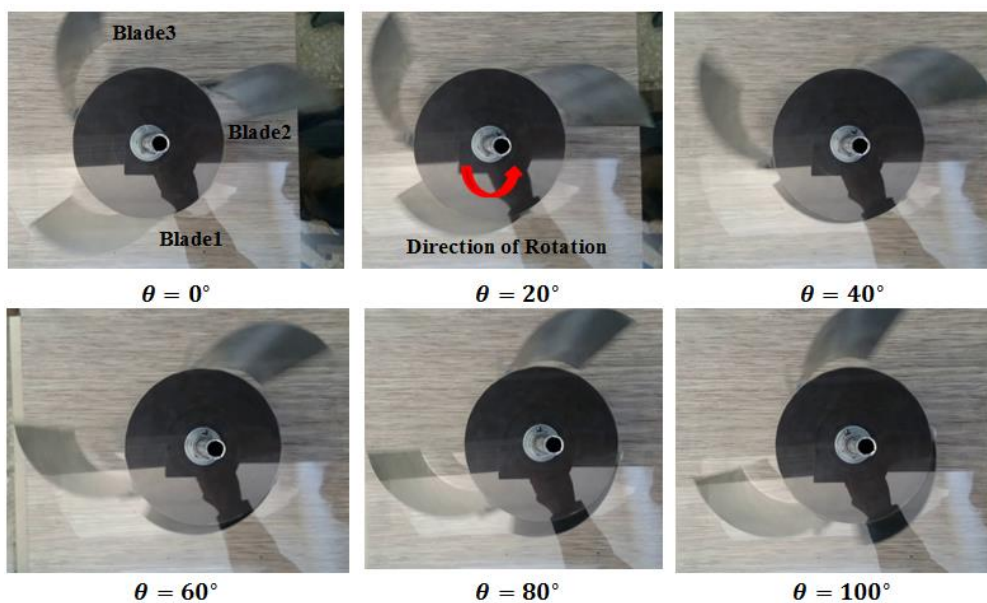**Fig. 7. Computational grid near the turbine blades.**

Fig. 8. Experimental snapshots for the blade positions in a cycle of rotation for the 3-bladed rotor with an aspect ratio of 2.0, at TSR=0.5.

high-speed imaging for a 6-bladed tidal current turbine at various rotational speeds. Their results, based on image processing, revealed that the all the opening processes initiate at about 90º and continues upto 120º. Furthermore, all the closing processes initiated at about 180º and ended up at about 360º. They also declared that these angular positions are almost independent of the TSR (Tip Speed Ratio), which is defined as presented in Eq. (6):

$$TSR = \frac{\omega R_c}{U} \qquad (6)$$

In a previous paper, Amiri *et al.* (2016) investigated the effects of blade numbers on the aerodynamic efficiency of a pivoted wind turbine, based on the opening/closing instances reported by (Yang and Lawn 2011). Their results showed that the 3-bladed rotor has a higher maximum power coefficient than the 4 and 6-bladed ones. Therefore, in this study, a 3-bladed rotor is selected as the main goal. In order to

determine the angular positions of the opening/closing processes in this turbine, high-speed imaging are performed using a SONY A6300 camera. The captured images for the rotor with the aspect ratio of 2.0, at TSR=0.5, are illustrated in Fig. 8 at various angular positions in one cycle. The 3-bladed rotor has three 120º cycles in one complete revolution. The observations revealed that the opening process begins at about 80º and ends up at 120º, while the closing process initiates at 300º and ends up at 40º. There might be several reasons for the difference between these observations and those in the experiments of (Yang and Lawn 2011). First, they have testes a 6-bladed rotor, however, a 3-bladed rotor is examined here. Furthermore, their experiments were performed in a water tunnel with a water velocity of about 0.65 *m/s*, while the experiments of the current study are performed in a wind tunnel with the wind velocities of about 9 *m/s*. As a result, in this study, the angular positions obtained based on the experimental images are used
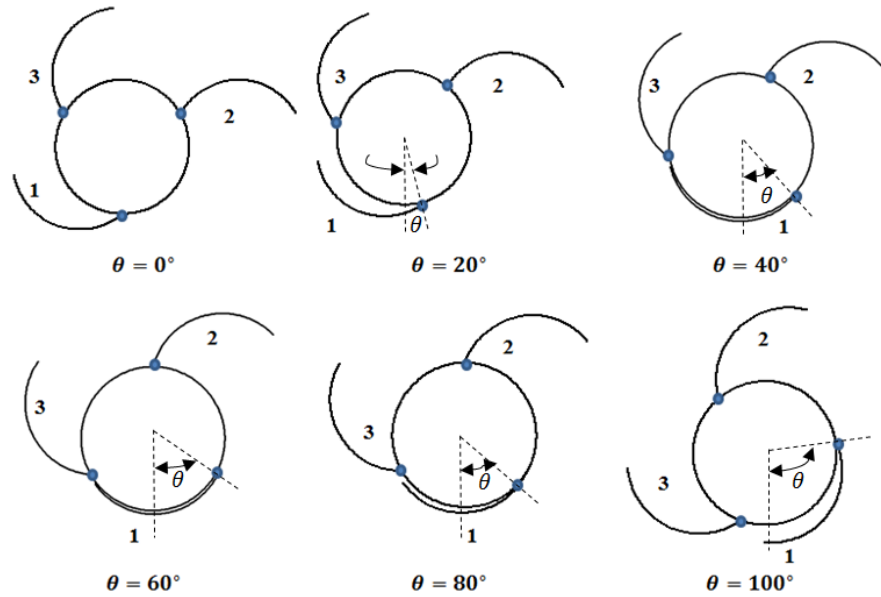
824

Fig. 9. Blade positions in a cycle of rotation for the 3-bladed rotor, based on the experimental observations given in Fig. 6.

in the numerical simulation of the wind rotor. The angular positions of the blades in one complete revolution of the rotor, used in the numerical simulations, are shown in Fig. 9.

In the numerical simulation of the wind rotors using the MRF model, the rotor has to be simulated in several quasi-steady angular positions in its cycle. The question is how many angular positions are required in the numerical simulation to accurately present the performance of the rotor. Therefore, in this study, numerical simulation are performed in two cases; a) with 6 angular positions and b) with 12 angular positions in one cycle. The simulations are carried out at the air velocity of 9 *m/s* (Reynolds number of 9.9×10^4). The resultant pressure distributions at TSR=0.5 are depicted in Fig. 10. TSR=0.5 is the dimensionless rotor angular velocity where the rotor maximum power coefficient has occured.

The opening/closing processes observed in the experiments can be explained using the numerical results. Blade 1 starts the opening process at $\theta=80°$ and continues up to $\theta=120°$, where the blade reaches its fully-opened status. The higher pressure in the concave side of this blade can be seen in Fig. 10. As Blade 1 opens, it acts as an obstacle in front of the wind and the wake formed behind it, lowers the positive torque of Blade 2. The onset of the closing process, however, occurs for Blade 3 at $\theta=60°$. The numerical results also confirm that the average pressure on the convex side of this blade becomes higher than its concave side at this angular position. At the end of the cycle, at $\theta=120°$, Blade 3 replaces Blade 1 and the rest of the closing process is experienced by Blade 1 up to $\theta=40°$.

The power and torque coefficients are commonly used to present the aerodynamic performance of the wind turbines, which are defined as given in Eqs. (7) and (8) (Yang and Lawn 2011):

$$C_P = \frac{2T\,\omega}{\rho U^3 \left(R_t + D/2\right)H} \tag{7}$$

$$C_M = \frac{2T}{\rho U^2 \left(R_t + D/2\right)HR_c} \tag{8}$$

where *T* is the torque and ω is the rotational speed.

The *TSR* can be used to link the power and torque coefficients as given in Eq. (9):

$$C_M = \frac{C_P}{TSR} \tag{9}$$

The flow Reynolds number, Re, for the turbine is calculated based on the drum diameter as written in Eq. (10):

$$Re = \frac{\rho U D}{\mu} \tag{10}$$

where U is the upstream wind velocity and μ is the air viscosity.

The numerical results for the angular variations of the total torque coefficient in one complete rotor revolution is depicted in Fig. 11 for the two cases; a) simulations with 6 rotor angular positions and b) with 12 angular positions in one cycle. This comparison is also made for the averaged power coefficient variations as a function of *TSR* in Fig. 12, where the experimental results are also presented for the rotor with the aspect ratio of 2.0. The numerical simulations are performed for 6 angular positions in one complete rotation and the total power coefficient of the turbine is calculated by averaging the values of these points(Yang and Lawn 2011).Both figures show that the difference between the two cases are negligible and hence, it seems adequate to consider 6 angular positions for the numerical simulations due to a considerable less computational cost.
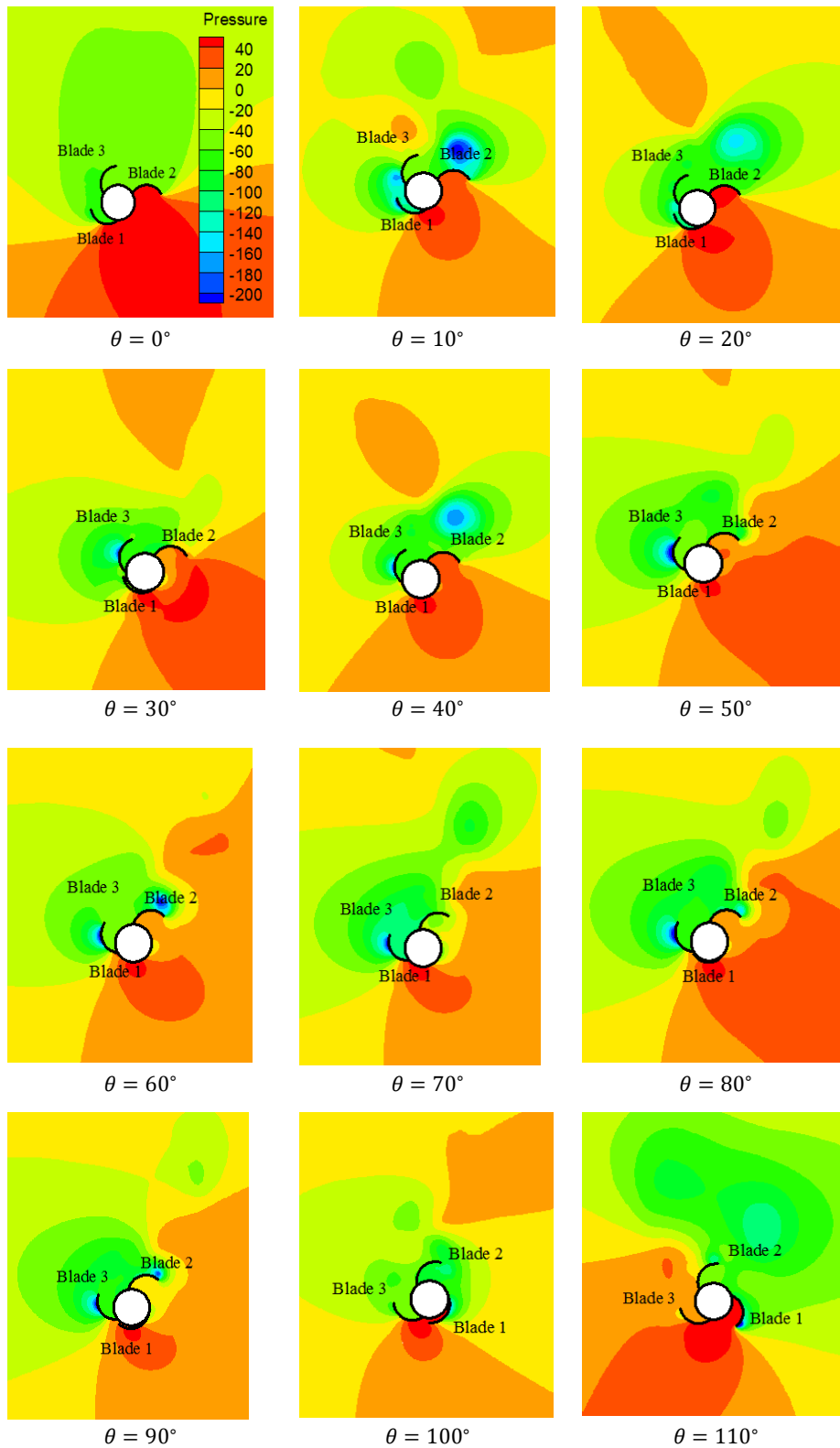
Fig. 10. Pressure contours (Pascal) for the 3-bladed rotor at *TSR*=0.5, for 12- angular positions.

As mentioned before, the numerical simulations of the current study are performed on a two-dimensional computational domain. However, three dimensional effects, especially at the blade tips, might deteriorate the validity of the numerical simulations. Nevertheless, the existence of the end plates at two ends of the turbine, can greatly restrict these three-dimensional effects. Furthermore, increasing the rotor aspect ratio can also weaken the effects of the blade tip vortices on the overall turbine efficiency. Therefore, a comparison is made between the two-dimensional numerical results with the experimental data of the rotors with various aspect ratios, both with and without the end plates. The

effects of adding end plates and increasing the rotor aspect ratio on the averaged torque and power coefficients are shown in Figs. 13 and 14, respectively. As the figures clearly show, increasing the aspect ratio has enhanced the total averaged torque and power coefficients at all TSRs. A similar trend can be observed for the effects of adding end plates. At each aspect ratio, adding end plates has greatly increased the rotor performance, due to a significant reduction of blade tip losses. Increasing the rotor aspect ratio and adding end plates, not only improves the maximum power coefficient, but also extends the working TSR of the turbine. As expected, the numerical results obtained on a two-dimensional computational domain, are appropriate for a rotor with an aspect ratio of infinity. This can be well observed in the figures that as the tip vortices are restricted by increasing the aspect ratio or adding end plates, the experimental data get closer to the numerical results. For the rotor with the aspect ratio of 2.0 with end plates, a satisfactory agreement exists between the numerical and experimental data. An important deduction of these figures is that two-dimensional numerical results are not comparable with the experimental data of the vertical axis wind turbines without end plates.
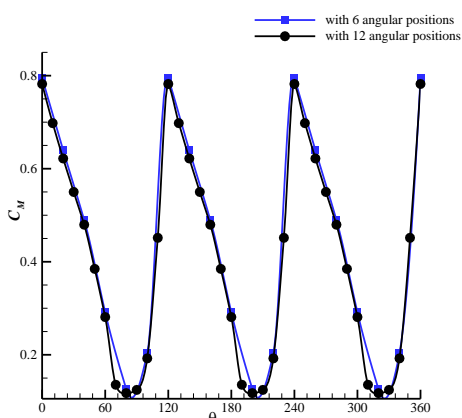

Fig. 11. Variations of the total torque coefficient, for the simulations performed with 6 and 12 angular positions in one complete rotor revolution at $TSR=0.5$.
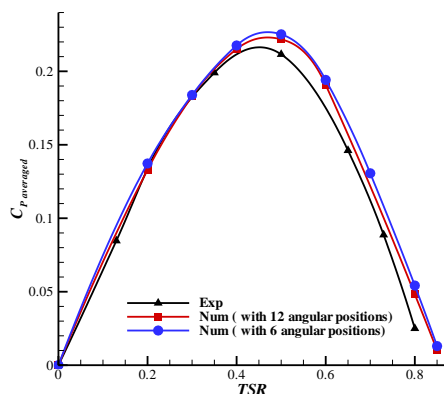

Fig. 12. Comparison of the numerical averaged power coefficients, $C_{P\_averaged}$, obtained with 6 and 12 angular positions in a rotor cycle with the experimental data.
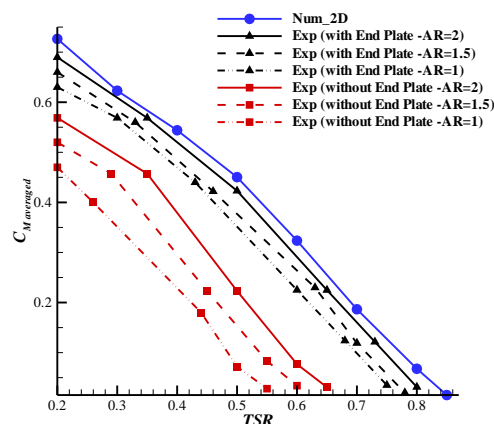

Fig. 13. Variations of the experimental averaged torque coefficients, for the 3-bladed rotor at various aspect ratios.
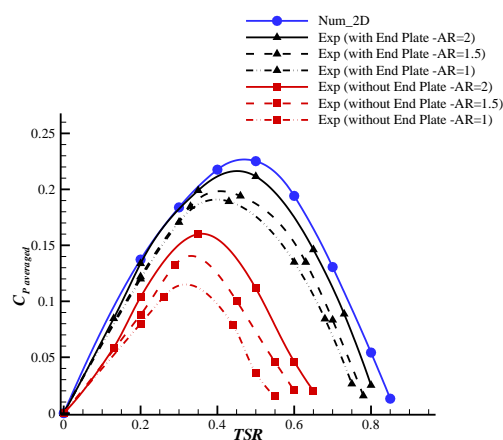

Fig. 14. Variations of the experimental averaged power coefficients, for the 3-bladed rotor at various aspect ratios.

6. CONCLUSION

In order to modify the low aerodynamic performance of the conventional Savonius rotor and also eliminate its negative torques in some angular positions, a novel three-bladed pivoted rotor is introduced and examined in details. The wind tunnel experiments are performed in a subsonic open-jet type wind tunnel. For the numerical simulations, however, Ansys-Fluent commercial software is employed, where the Multiple Reference Frame model (MRF) and the SST k-ω turbulence model are used. The effects of adding end plates and the rotor aspect ratio on the turbine torque and power coefficients are studied in details. The main findings of the present study can be summarized as follows:

✓ The pivoted wind turbine with and without endplates has no negative torque in one complete rotor revolution.

✓ Adding end plates at the two ends of the turbine, greatly increases the torque and power coefficients of the turbine. For example for a rotor with an aspect ratio of 2.0, adding end plates results in a 31% increase in the maximum

power coefficient of the turbine.

✓ The rotors with end plates have a greater working TSR in comparison with those without end plates.

✓ Increasing rotor aspect ratio, has similar effects to those of adding end plates. In other words, a rotor with a larger aspect ratio has a larger maximum power coefficient and also a greater working range of TSR. In fact, increasing the rotor aspect ratio weakens the effects of the blade tip vortices on the overall turbine efficiency.

✓ Two dimensional numerical simulations correspond to a wind rotor having an infinite aspect ratio. Comparing numerical results with the experimental data revealed that the numerical results are in a good agreement with the experimental data of a wind rotor with an aspect ratio of 2.0 equipped with end plates. In other words, two-dimensional numerical results are not comparable with the experimental data of the wind rotors having aspect ratios lower than 2.0, without end plates.

✓ For the numerical simulations using the MRF model, it is necessary to determine how many angular positions are required to accurately model the rotor in one cycle. The results of the current study show that considering 6 angular positions in one cycle will provide reasonable results in comparison with the experimental data.

✓ A summary of the numerical and experimental results are given in Table 3.

As the future works, the following suggestions can be considered for further studies:

✓ At small rotor aspect ratios, three dimensional effects cannot be neglected. Therefore, performing three dimensional numerical simulations can better reveal the flow physics around this type of turbines.

✓ Instead of using pivoted blades, automatic valves can be devised on the blades with various sizes and positions, which might lead to higher power coefficients and a simpler design.

REFERENCES

Alexander, A. J. and B. P. Holownia (1978). Wind tunnel tests on a savonius rotor. *Journal of Wind Engineering and Industrial Aerodynamics* **3**(4), 343-351.

Altan, B. D. and M. Atılgan (2010). The use of a curtain design to increase the performance level of a Savonius wind rotors. *Renewable Energy* **35**(4), 821-829.

Amiri, M., A. R. Teymourtash and M. Kahrom (2016). Experimental and numerical investigations on the aerodynamic performance of a pivoted Savonius wind turbine. *Proceedings of the Institution of Mechanical Engineers, Part A: Journal of Power and Energy* 231(2): 87-101.

Anbarsooz, M. (2016). Aerodynamic performance of helical Savonius wind rotors with 30° and 45° twist angles: Experimental and numerical studies. *Proceedings of the Institution of Mechanical Engineers, Part A: Journal of Power and Energy* 230(6), 523-534.

Ansys Inc., A. (2009). Ansys Fluent 15.0 Theory Guide, Ansys, Inc.

Chan, C. M., H. L. Bai and D. Q. He (2018). Blade shape optimization of the Savonius wind turbine using a genetic algorithm. *Applied Energy* 213, 148-157.

D'Alessandro, V., S. Montelpare, R. Ricci and A. Secchiaroli (2010). Unsteady Aerodynamics of a Savonius wind rotor: a new computational approach for the simulation of energy performance. *Energy* 35(8), 3349-3363.

Duffett, I., J. Perry, B. Stockwood and J. Wiseman (2009). Design and Evaluation of Twisted Savonius Wind Turbine." BSc Thesis, Mechanical Engineering Department, Memorial University of Newfoundland, Canada.

El-Askary, W. A., M. H. Nasef, A. A. AbdEl-hamid and H. E. Gad (2015). Harvesting wind energy for improving performance of Savonius rotor. *Journal of Wind Engineering and Industrial Aerodynamics* 139(0), 8-15.

Emmanuel, B. and W. Jun (2011). Numerical Study of a Six-Bladed Savonius Wind Turbine. *Journal of Solar Energy Engineering* 133(4), 044503-044503.

Ghatage, S. V. and J. B. Joshi (2012). Optimisation of vertical axis wind turbine: CFD simulations and experimental measurements. *The Canadian Journal of Chemical Engineering* 90(5), 1186-1201.

Hayashi, T., Y. Li, Y. Hara and K. Suzuki (2005). Wind Tunnel Tests on a Different Phase Three-Stage Savonius Rotor. *JSME International Journal Series B Fluids and Thermal Engineering* 48, 9-16.

Kamoji, M. A., S. B. Kedare and S. V. Prabhu (2009). Performance tests on helical Savonius rotors. *Renewable Energy* 34(3), 521-529.

Kang, C., H. Liu and X. Yang (2014). Review of fluid dynamics aspects of Savonius-rotor-based vertical-axis wind rotors. *Renewable and Sustainable Energy Reviews* 33(0), 499-508.

Kianifar, A. and M. Anbarsooz (2011). Blade curve influences on the performance of Savonius rotors: experimental and numerical. *Proceedings of the Institution of Mechanical Engineers, Part A: Journal of Power and Energy* 225, 343-350.

Lanzafame, R., S. Mauro and M. Messina (2013). Wind turbine CFD modeling using a correlation-based transitional model. *Renewable Energy* 52(0), 31-39.

Moffat, R. J. (1982). Contributions to the Theory of

Single-Sample Uncertainty Analysis. *Journal of Fluids Engineering* 104(2), 250-258.

Moffat, R. J. (1988). Describing the uncertainties in experimental results. *Experimental Thermal and Fluid Science* 1(1), 3-17.

Nasef, M. H., W. A. El-Askary, A. A. AbdEl-hamid and H. E. Gad (2013). Evaluation of Savonius rotor performance: Static and dynamic studies. *Journal of Wind Engineering and Industrial Aerodynamics* 123, Part A(0): 1-11.

Pope, K., V. Rodrigues, R. Doyle, A. Tsopelas, R. Gravelsins, G. F. Naterer and E. Tsang (2010). Effects of stator vanes on power coefficients of a zephyr vertical axis wind turbine. *Renewable Energy* 35(5), 1043-1051.

Ricci, R., R. Romagnoli, S. Montelpare and D. Vitali (2016). Experimental study on a Savonius wind rotor for street lighting systems. *Applied Energy* 161, 143-152.

Roy, S. and U. K. Saha (2013a). Computational Study to Assess the Influence of Overlap Ratio on Static Torque Characteristics of a Vertical Axis Wind Turbine. *Procedia Engineering* 51(0), 694-702.

Roy, S. and U. K. Saha (2013b). Review on the numerical investigations into the design and development of Savonius wind rotors. *Renewable and Sustainable Energy Reviews* 24(0), 73-83.

Roy, S. and U. K. Saha (2015). Wind tunnel experiments of a newly developed two-bladed Savonius-style wind turbine. *Applied Energy* 137(0), 117-125.

Saha, U. K., S. Thotla and D. Maity (2008). Optimum design configuration of Savonius rotor through wind tunnel experiments. *Journal of Wind Engineering and Industrial Aerodynamics* 96(8–9), 1359-1375.

Tang, Z., Y. Yao, L. Zhou and B. Yu (2013). A review on the new structure of Savonius wind turbines. *Advanced Materials Research* 608-609, 467-478.

Tian, W., Z. Mao, B. Zhang and Y. Li (2018). Shape optimization of a Savonius wind rotor with different convex and concave sides. *Renewable Energy* 117(Supplement C): 287-299.

Torresi, M., B. Fortunato, G. Pascazio and S. M. Camporeale (2011). CFD Analysis of a Savonius Rotor in a Confined Test Section and in Open Field. Volume 1: Aircraft Engine; Ceramics; Coal, Biomass and Alternative Fuels; Wind Turbine Technology.

Yang, B. and C. Lawn (2011). Fluid dynamic performance of a vertical axis turbine for tidal currents. *Renewable Energy* 36(12), 3355-3366.